ELSEVIER

Surface Science 370 (1996) 32–46

surface science

Bromine adsorption, reaction, and etching of Cu(100)

C.Y. Nakakura [a], E.I. Altman [b,*]

[a] *Department of Applied Physics, Yale University, New Haven, CT 06520, USA*
[b] *Department of Chemical Engineering, Yale University, New Haven, CT 06520, USA*

Received 28 March 1996; accepted for publication 9 July 1996

Abstract

The interaction of Br_2 with Cu(100) was characterized using temperature-programmed desorption (TPD) and low-energy electron diffraction (LEED). Initial exposure to Br_2 resulted in the formation of a c(2×2) LEED pattern and CuBr desorption peaks at 870 and 1000 K. These desorption peaks saturated at a dose of approximately 5 L and were attributed to Br chemisorption. Continued exposure to Br_2 resulted in the growth of Cu_3Br_3 desorption peaks associated with the formation of bulk CuBr. The Cu_3Br_3 desorption peaks exhibited a strong coverage dependence. At low CuBr coverages, desorption peaks at 450 and 485 K were observed, while at intermediate coverages a third peak at 540 K was observed, and at high coverages a single broad peak at 500 K was observed. Similar results were obtained whether the CuBr layer was formed by exposure to Br_2 or by deposition of Cu_3Br_3 onto a c(2×2) layer. The two higher-temperature peaks were shown to be consistent with sublimation of α and β CuBr, while the lowest-temperature peak could not be associated with sublimation of any bulk phase of CuBr. The lowest-temperature peak was attributed to either a grain-size effect or to the interaction of CuBr with chemisorbed Br. At 325 K, growth of CuBr resulted in a hexagonal LEED pattern that disappeared upon annealing to 400 K. Again, the same results were obtained for CuBr formed by reaction with Br_2 and by vapor deposition of Cu_3Br_3, suggesting that the reaction produces near-equilibrium structures. The hexagonal LEED pattern was attributed to compressed epitaxial CuBr(111). The reaction of Br_2 with Cu(100) was characterized by a constant sticking coefficient, indicating that the reaction is adsorption-rate limited over the range studied. The sticking coefficient was found to depend on temperature in two distinct ways: (i) annealing the c(2×2) layer irreversibly increases the sticking coefficient, and (ii) the sticking coefficient reversibly decreases with increasing reaction temperature. The first effect was attributed to structural changes in the chemisorbed layer.

Keywords: Adsorption kinetics; Bromine; Chemisorption; Compound formation; Copper; Corrosion; Etching; Evaporation and sublimation; Halides; Halogens; Low energy electron diffraction (LEED); Low index single crystal surfaces; Molecule–solid reactions; Oxidation; Thermal desorption spectroscopy

1. Introduction

Etching reactions of metals are used to define patterns for gates and interconnects in integrated circuits. Aluminum is currently used as the interconnect material in nearly all integrated circuits [1,2]. Alternative materials with lower resistivity are being sought because RC (resistance–capacitance) time delays in Al interconnects will soon limit the speed of integrated circuits [1,3]. Much attention has been given to copper as a replacement material because of its low resistivity and its resistance to electromigration [3]. The lack of low-temperature dry-etching processes for Cu has delayed the introduction of devices with Cu interconnects (Etching temperatures must be kept low to prevent degradation of polymer etch

* Corresponding author. Fax: +1 203 4327232; e-mail: eric.altman@yale.edu

PII S0039-6028(96)00950-8

masks and to limit interdiffusion of circuit components [1–3]). Therefore, we recently started a project aimed at elucidating the atomic-scale mechanisms of etching reactions of metal surfaces. The long-term goal of the project is to use the detailed understanding of the etching mechanism to help develop low-temperature dry etching processes for Cu. We have begun this project by characterizing the adsorption, reaction, and etching of Cu surfaces by bromine.

Copper etching by chlorine with and without plasmas has been studied previously [4–6]. Winters et al. [4,5] showed that although plasma etching is commonly used in industry, the energetic ions generated by the plasma actually inhibit etching of many metals, including Cu. Therefore, only atomic and molecular species need be considered in modeling etching of Cu surfaces by halogens. Previous studies also showed that when a Cu(100) surface is exposed to Cl_2 at room temperature, a chemisorbed layer of Cl atoms rapidly forms [6]. After the chemisorbed layer is saturated, the Cl_2 sticking coefficient decreases by several orders of magnitude but does not go to zero. Rather, continued exposure results in the formation of CuCl. The CuCl can then be sublimed by heating to approximately 470 K. Since the subliming species contains Cu, the surface is etched. Less work has been reported for the Br_2–Cu system; however, the results that have been published indicate that Br_2 behaves qualitatively similar to Cl_2 on Cu(100) [7,8]. Photoemission studies revealed that Br_2 initially dissociates on Cu surfaces to form a chemisorbed layer of Br atoms that saturates after a dose of roughly 2.5 L [8]. Continued exposure to Br_2 results in the growth of CuBr [7,8]. Thus a general picture of Cu etching by halogens as a two-step process emerges, the two steps being (i) halogenation to form bulk Cu halide and (ii) sublimation of the copper halide.

Although the general etching mechanism is known, important aspects of the individual reaction steps remain poorly characterized. For the halogenation step there have been conflicting reports in the literature regarding the crystal-plane anisotropy of CuCl formation. One group [7] has suggested that polycrystalline Cu samples (presumed to be mostly (111)-oriented) may be largely unreactive once the chemisorbed layer is saturated, while another [9] reports the formation of thick CuCl layers regardless of the orientation of the Cu surface. In addition, for Cl_2 on Cu(100) the CuCl formation rate has been observed to decrease with increasing temperature [6]. Such decreases in reaction rate with temperature are common for oxidation reactions, but remain poorly understood [10–17]. Whatever the origin of the temperature dependence, the decrease in chlorination rate with temperature has important implications for the etching process. The mechanism outlined above suggests that the etching temperature is limited by the vapor pressure of the copper halide. Under steady-state conditions, however, the etching rate of Cu by Cl_2 has been found to be much lower than the sublimation rate of CuCl, suggesting that under reaction conditions chlorination may be rate-limiting [6]. Thus, increasing the volatility of the subliming species may not be sufficient to achieve high steady-state etching rates at lower temperatures. Aspects of the halide-removal step have also not been characterized. It has been suggested that etching temperatures can be reduced by limiting the halide grain size [18,19]. Small halide crystallites are expected to sublime at lower temperatures because they have a higher density of subliming units at edge and corner sites that are bound to fewer neighbors, and thus may require less energy to remove [10]. There have been no experimental measurements of the magnitude of this effect for copper halides.

To begin addressing the issues described above, the reaction of Cu(100) with Br_2 to form CuBr and the subsequent removal of CuBr by sublimation were systematically studied using temperature-programmed desorption (TPD) and low-energy electron diffraction (LEED). Bromine was selected because previous studies indicated that Br_2 is more reactive towards Cu than Cl_2 [7]. Thus lower Br_2 doses are required to form halide multilayers, making Cu etching by Br_2 more amenable to study with ultra-high vacuum (UHV) techniques. In this paper, it will be shown that reaction of Br_2 with Cu(100) below 365 K results in the formation of an epitaxial (111) compressed CuBr layer atop a $c(2\times2)$ chemisorbed Br layer. The same epitaxial relationship was observed when CuBr was sub-

limed onto a chemisorbed Br layer suggesting that the reaction of Br_2 with Cu produces near-equilibrium structures. Two distinct temperature effects on the CuBr formation rate were observed: (i) an irreversible increase in the halide-formation rate after annealing the chemisorbed layer and (ii) a reversible decrease in the halide-formation rate that depends solely on the surface temperature during reaction. The first effect is attributed to an irreversible structural change in the chemisorbed layer. The sublimation of CuBr was observed to depend on the CuBr coverage. Limiting the CuBr coverage resulted in a low-temperature desorption peak, while high coverages yielded a zero-order desorption peak with a heat of sublimation consistent with CuBr. Again, similar results were obtained for CuBr formed by reaction with Br_2 and for CuBr sublimed onto a chemisorbed Br layer. The low-temperature peak is due to either the size effect described above or due to the interaction of CuBr with chemisorbed Br atoms. In either event, the results demonstrate that for Cu etching by Br_2, etching temperatures can be reduced by limiting the thickness of the halide layer.

2. Experimental

The TPD and LEED experiments were performed using a stainless steel UHV system equipped with LEED optics, a double-pass cylindrical mirror analyzer for Auger electron spectroscopy (AES), a sputter-ion gun, a quadrupole mass spectrometer (UTI 100C-12), and a scanning tunneling microscope. Pumping was provided by a 300 l s^{-1} ion pump and a small turbomolecular pump used to remove sputter gases from the chamber. The base pressure of the system is 1×10^{-10} Torr. For the experiments described in this paper, a Br_2 source (described below) and a CuBr evaporator were added to the system. The CuBr evaporator consisted of a resistively heated Ta envelope filled with CuBr powder. After extensive outgassing, CuBr was sublimed onto the sample by heating the envelope to 485 K.

The Cu(100) sample (7 mm diameter disc, 0.5 mm thick) was spot-welded to a 0.025 mm thick Cu foil of the same diameter. The sample was heated via conduction from resistively heated Ta leads spot-welded to the foil. A chromel–alumel thermocouple spot-welded to the back of the foil was used to measure the sample temperature. Prior to each TPD series, the sample was sputter-cleaned with 0.5 keV Ar^+ ions for repeated cycles (15 min at 675 K, 15 min at 875 K) until no impurities were observed by AES. The sample was then annealed at 920 K for 5 min and slowly cooled to remove sputter damage. This procedure yielded a sharp (1×1) LEED pattern.

For TPD and LEED experiments, Br_2 was generated in situ using a solid-state electrochemical cell. A similar approach has been used to study etching of semiconductor surfaces [20]. As described by Spencer et al. [21], Br_2 is formed at the Pt anode of a Cd^{2+}-doped AgBr electrochemical cell. In our arrangement, the glass tube housing the electrochemical cell narrows to a 2 mm diameter capillary at the end thus collimating the emerging Br_2 gas. During dosing, the sample was positioned within a few mm of the end of the capillary. For the electrochemical cell, the gas dose is proportional to the electrochemical current times the exposure time; thus doses are reported in units of μA s. The dose in Langmuirs was estimated by comparing the time required to achieve a certain coverage (as determined by the TPD peak area) with the sample turned away from the doser with the time required with the sample positioned in front of the doser. If the pressure rise in the system is due solely to Br_2, we find that 80 μA s is equivalent to 1 L and that the effective Br_2 pressure at the doser is 280 times the background pressure. This gives effective Br_2 pressures during dosing between 6×10^{-8} and 3×10^{-7} Torr. These values, however, are only approximate because it has been shown that halogens react with the stainless steel walls of vacuum chambers to produce HX [22], and mass spectra of our UHV system did in fact reveal significant amounts of HBr. It should be noted that when the sample is positioned in front of the doser, the Br_2 gas can contact only the Pt anode and the glass walls of the electrochemical cell before reaching the sample; thus, reaction of Br_2 with the vacuum chamber walls does not influence our results.

Because Br_2 reacts with the walls of the vacuum chamber, and because the other expected desorp-

tion products (CuBr and Cu_3Br_3) are non-volatile, TPD experiments were performed with the sample positioned within a few cm of the ionizer of the mass spectrometer. Desorbing CuBr and Cu_3Br_3 not detected by the mass spectrometer were presumed to condense on the chamber walls, thus the measurements are line-of-sight. Custom software was used to control the temperature ramp, switch the mass spectrometer to different masses, and collect the data. With this setup the number of masses that can be monitored during a TPD run is limited only by the switching time of the mass spectrometer. For the work described in this paper, a heating rate of 7 K s^{-1} was used and five masses were monitored.

The vapor phase species in equilibrium with CuBr is Cu_3Br_3 [23]. The most abundant isotope of Cu_3Br_3 has a mass of 432 amu, which is beyond the 400 amu limit of the mass spectrometer used in this study. Therefore, to determine the cracking pattern of Cu_3Br_3, thick CuBr films were sublimed towards the ionizer of the mass spectrometer. Fig. 1 shows a typical mass spectrum. The dominant peaks are due to Cu^+ at 63 and 65 amu, Br^+ at 79 and 81 amu (with HBr^+ at 80 and 82 amu), $CuBr^+$ at 142, 144, and 146 amu, Cu_2Br^+ at 205, 207, 209 and 211 amu, and $Cu_3Br_2^+$ at 347, 349, 351, 353, 355, and 357 amu. Because of the limited switching speed of the mass spectrometer, not all of these masses could be monitored during a TPD run. The masses selected for the TPD experiments described in this paper were Cu at 63 or 65 amu, CuBr at 142 and 144 amu, Cu_3Br_2 at 349 amu, and either Br_2 at 160 amu or Br at 79 amu. Although Fig. 1 indicates that the Cu_2Br signal is more intense than the Cu_3Br_2 signal, Cu_3Br_2 was chosen because it is indicative of a species containing at least three Cu atoms, thereby increasing our confidence in the assignment of desorption peaks to Cu_3Br_3 rather than to smaller CuBr clusters. We did perform some TPD experiments with polycrystalline Cu monitoring Cu_2Br at 209 amu, and found that the Cu_2Br intensity tracked the intensity of the other Cu_3Br_3 fragments.

3. Results

3.1. Desorption and etching

Temperature-programmed desorption results revealed desorption in two temperature ranges. As shown in Fig. 2 for a dose of 1500 μA s, at temperatures above 700 K CuBr is the only observed desorbing species; the increase in the Cu signal at high temperatures is due to sublimation of the Cu substrate. Fig. 2 also shows that no molecular Br_2 desorbs from the surface. This indicates that adsorption of Br_2 is dissociative and irreversible, since Br_2 is not completely cracked in the mass spectrometer and so Br_2 desorption would create a signal at 160 amu. We also monitored atomic Br and found no evidence of desorption of atomic Br. This contrasts with previous studies of Cl_2 chemisorption on Cu surfaces that suggested that atomic Cl was the predominant desorbing species [24]. Below 600 K, Cu, CuBr and Cu_3Br_2 were observed in proportions consistent with the cracking pattern of Cu_3Br_3 shown in Fig. 1. Also notice that below 600 K the desorption peaks for the different masses track one another, suggesting a common parent for each of the species. Thus desorption below 600 K is attributed to Cu_3Br_3 and is associated with sublimation of CuBr. In the remainder of this paper the TPD data will be presented as the sum of the Cu, CuBr and Cu_3Br_2 traces below 650 K. Above 650 K, the TPD data will be presented as the sum of the two CuBr traces, the only species observed to desorb at these temperatures, excluding sublimation of the substrate.

Fig. 3 illustrates the evolution of the TPD curves as a function of Br_2 exposure with the sample at 325 K. At low exposures, the TPD curves are dominated by overlapping CuBr desorption peaks at 870 and 1000 K. As shown in Fig. 3, these peaks fill sequentially and are saturated by doses exceeding 400 μA s, or approximately 5 L. The high desorption temperatures and the high sticking coefficient are characteristic of the chemisorption of reactive species on metal surfaces, and thus the high-temperature peaks are attributed to Br_2 chemisorption on Cu(100). Continued exposure to Br_2 results in the slow growth of Cu_3Br_3 desorption features between 400 and 515 K. As shown in Fig. 3, desorption in this regime varies dramatically with Br_2 exposure. At a dose of 1500 μA s, desorption peaks at 450 and 485 K are observed. When the exposure is increased to 5000 μA s, the peak at 450 K shifts to higher temperatures and a third desorption peak at 540 K appears (seen more

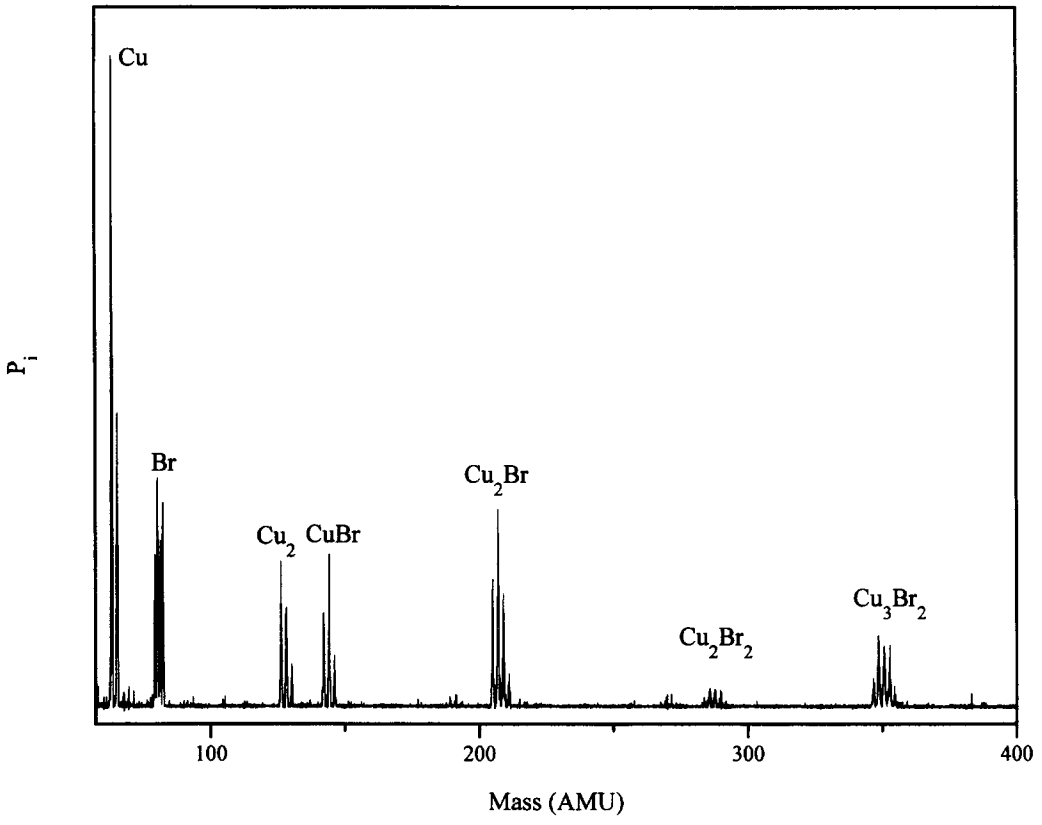

Fig. 1. Mass spectrum of vapor-phase CuBr illustrating the cracking pattern of Cu_3Br_3. The spectrum was obtained by subliming thick CuBr films towards the ionizer of the mass spectrometer. An ionizing electron energy of 70 eV was used to ionize the gas-phase species.

clearly in Fig. 5a). Increasing the exposure further causes the lowest-temperature peak to disappear and the two higher-temperature peaks to merge into a single broad peak; continued exposure simply causes the intensity of this remaining peak to grow. Again, the ratios of Cu, CuBr and Cu_3Br_2 are consistent with the cracking pattern of Cu_3Br_3, the species known to sublime from CuBr. This suggests that the desorption features below 600 K are indicative of reaction of Br_2 with Cu to form bulk CuBr. The desorption peaks, however, appear to be far more complex than one would expect for a simple sublimation process.

Sublimation is a zero-order process. For TPD, this means that as long as the surface area of the subliming species is constant, or the coverage of the bulk species (in this case CuBr) is greater than 1 ML, the TPD curve simply reflects the vapor pressure of the subliming species as a function of temperature [25]. Thus for starting coverages in excess of a monolayer, the leading edges of zero-order desorption curves are independent of initial coverage. During a TPD experiment the subliming material is eventually exhausted, causing the desorption rate to fall, resulting in a peak. The higher the initial coverage the longer it takes to exhaust the material; therefore, zero-order TPD peaks shift to higher temperature with increasing initial coverage.

The high-exposure data in Fig. 3 are consistent with zero-order kinetics. When the desorption curves are placed on top of one another, the leading edges coincide and the desorption peak shifts to higher temperatures. Further, as shown in Fig. 4, plotting the leading edges of the high-exposure TPD curves as the log of the mass

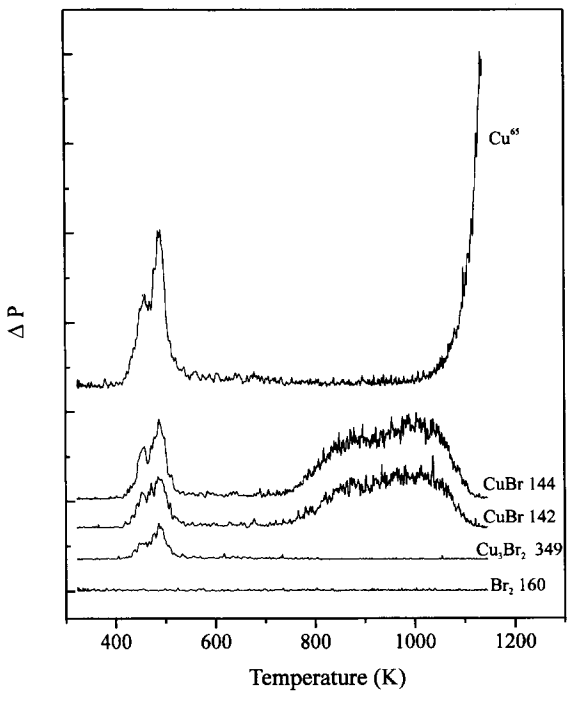

Fig. 2. Typical TPD traces for Cu(100) exposed to Br_2. These data are for a 1500 μA s dose at a temperature of 325 K. The background pressures of all the masses monitored are essentially zero, the data have been offset so the different traces do not overlap. Although Cu^{65} is less abundant than Cu^{63}, Cu^{65} was sometimes monitored to prevent the Cu signal from saturating the mass spectrometer amplifier.

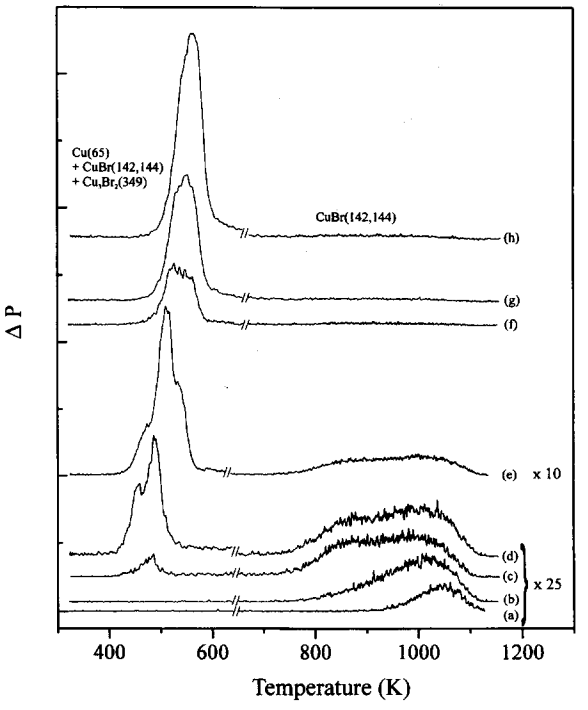

Fig. 3. Series of TPD curves for Br_2 reacted with Cu(100) at 325 K for the following doses: (a) 50, (b) 150, (c) 600, (d) 1·500, (e) 5·000, (f) 20·000, (g) 30·000, and (h) 40000 μA s. Below approximately 650 K the data are taken as the sum of the Cu, CuBr, and Cu_3Br_2 traces, while above 650 K, the data corresponds to the sum of the two CuBr traces; the slashes in the figure mark the switchover points. Data acquired at a heating rate of 7 K s^{-1}.

spectrometer signal versus $1/T$ yields a linear plot. The slope of the line indicates a heat of sublimation of 27.9 kcal mol^{-1}. Copper(I) bromide forms three phases: (i) an α phase (CsCl structure) with a heat of sublimation of 28.8 ± 0.9 kcal mol^{-1}, (ii) a β phase (wurtzite structure) with a heat of sublimation of 30.9 ± 0.9 kcal mol^{-1}, and (iii) a γ phase (zinc blende structure) with a heat of sublimation of 35.5 ± 0.9 kcal mol^{-1} [23]. The heat of sublimation obtained from the TPD data is within experimental error of the value for the α phase (a similar analysis of the sublimation of the Cu surface observed in Fig. 2 yielded a heat of sublimation of 75.8 kcal mol^{-1} compared to the accepted value of 79.1 ± 1.0 kcal mol^{-1}). This suggests that the subliming CuBr is in the α and/or β phases; γ-CuBr would lead to desorption-peak temperatures well above those observed. The broadness of the peak and the distinct peak at 540 K observed for a dose of 5000 μA s can be accounted for by a surface containing a mixture of the α and β phases. As shown in Fig. 5 for a dose of 20 000 μA s, the desorption curves can be fit by two zero-order desorption curves with heats of sublimation of 28.8 and 30.9 kcal mol^{-1}. The deconvolution of the peaks suggests an α/β ratio in the film of about 1.0. In the bulk, at temperatures below 660 K the γ phase is favored. Low-energy electron diffraction studies, to be described in detail below, suggest that formation of the α and β phases is not due to kinetic constraints during growth, but rather due to surface and interfacial energies altering the stability of the different phases.

While the desorption peaks observed at intermediate and high Br_2 exposures can be explained in terms of sublimation of different CuBr phases, the

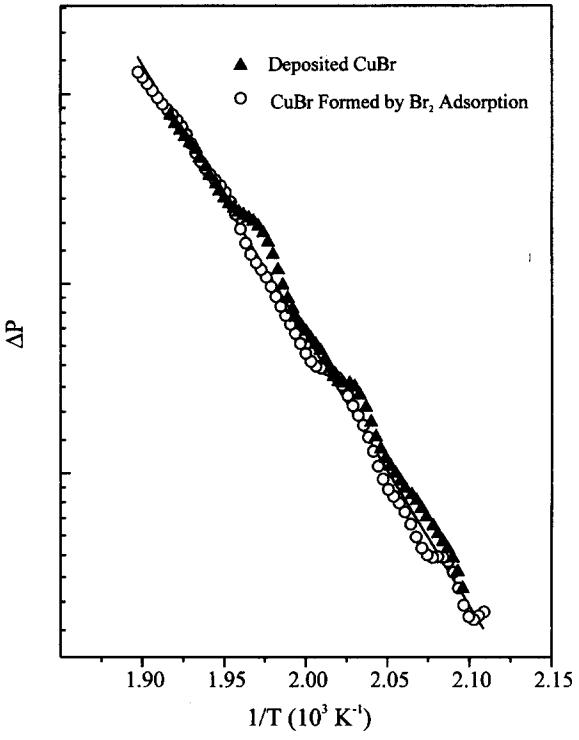

Fig. 4. Arrhenius plot of the log of the sum of the mass spectrometer signals at 65, 142, 144, and 349 amu versus $1/T$. The data were taken from the leading edges of the desorption curves for deposited CuBr and for CuBr formed by reaction of Br_2 with Cu(100) at 325 K. The slope of the line yields $\Delta H^{sub} = 27.9$ kcal mol^{-1}.

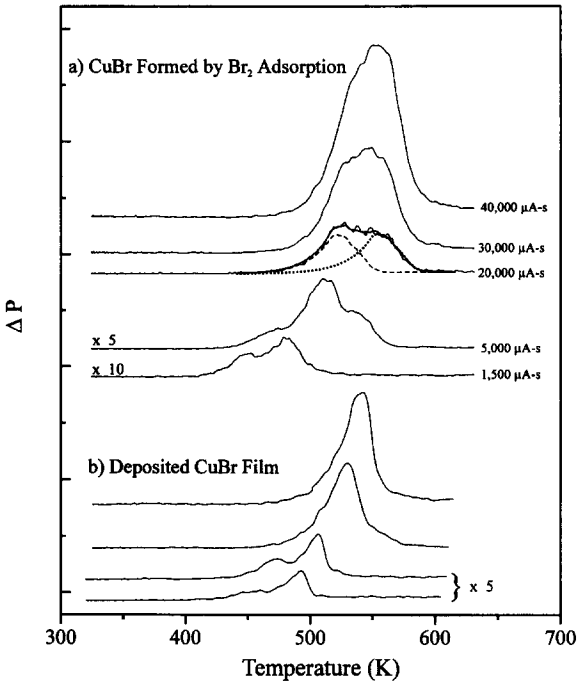

Fig. 5. Comparison of desorption curves for (a) CuBr formed by Br_2 adsorption at 325 K and (b) CuBr film deposited onto a chemisorbed Br layer. The lowest-temperature peak is seen in both cases at low coverages. For a 20 000 μA s dose, the desorption curve was deconvoluted into peaks due to α-CuBr ($\Delta H^{sub} = 28.8$ kcal mol^{-1}, dashed line) and β-CuBr ($\Delta H^{sub} = 30.9$ kcal mol^{-1}, dotted line). The solid line overlapping the data represents the sum of the two peaks.

desorption peak at 450 K cannot be associated with sublimation of any known phase of bulk CuBr. To attempt to determine the origin of this low-temperature desorption peak, we formed a model CuBr layer by subliming Cu_3Br_3 on top of a layer of chemisorbed Br atoms on Cu(100). The chemisorbed layer was formed by adsorbing 10–15 L of Br_2 and then annealing to 600 K to depopulate all low-temperature desorption peaks. The TPD results for the model layer are compared with results for similar Cu_3Br_3 coverages obtained by dosing with Br_2 in Fig. 5. Notice that the same low-temperature desorption peak is observed in both cases. Also notice that in both cases the low-temperature peak shifts to higher temperatures and eventually disappears when the coverage is increased. These results demonstrate that the low-temperature desorption peak is also due to sublimation of CuBr. Thus the general model of the interaction of Br_2 with Cu(100) is similar to that of Cl_2: short exposures result in the formation of a strongly bound chemisorbed layer, longer exposures result in the growth of a halide layer that can be removed by sublimation.

Since the lowest-temperature peak is only observed at the lowest CuBr coverages, it can be explained in terms of weaker interactions between Cu_3Br_3 and adsorbed Br atoms than between Cu_3Br_3 and bulk CuBr. The weaker interaction between the Cu_3Br_3 and the adsorbed Br atoms would be expected to persist to higher coverages. Temperature-programmed desorption, however, would not be sensitive to this effect at higher coverages because the surface layers would desorb first and these would initially be in contact with bulk CuBr; only when the last CuBr layer is

exposed would the desorption rate increase. Therefore, for high initial CuBr coverages, the rate increase would occur at a temperature above the bulk sublimation temperature, and no lower-temperature desorption peak would be observed. Alternatively, the low-temperature peak can also be explained in terms of the size effects described in Section 1. That is, thin CuBr films are expected to be made up of smaller CuBr crystallites than thicker films. A low-temperature desorption peak was also observed in a study of AgCl deposited atop a chemisorbed Cl layer on Ag(100), and was attributed to small AgCl crystallites on the surface [10]. The small crystallites contain a higher density of subliming units at corner and edge sites that are bound to fewer neighbors, and thus are expected to require less energy to sublime. Scanning tunneling microscopy studies are planned to distinguish these two effects.

Fig. 5 also shows other similarities between CuBr layers formed by reaction of Cu with Br_2 and layers formed by sublimation of Cu_3Br_3 onto a chemisorbed Br layer. At high coverages the leading edges of the desorption curves are identical. This is shown more clearly in Fig. 4 where the data are plotted as the log of the mass spectrometer signal versus $1/T$. This indicates that at desorption temperatures, both sublimed CuBr films and CuBr films formed by reaction of Cu with Br_2 contain significant amounts of α-CuBr and/or β-CuBr that are not normally stable at these temperatures. Fig. 5 also shows that desorption of CuBr formed by reaction of Cu with Br_2 results in broader desorption peaks, suggesting that CuBr formed by reaction of Cu with Br_2 may contain more of the β phase at desorption temperatures. This difference is due, at least in part, to annealing the chemisorbed layer; when an annealed chemisorbed surface is exposed to Br_2 the sublimation peak narrows considerably.

3.2. LEED

Low-energy electron diffraction was used to study the macroscopic order of Cu(100) surfaces exposed to Br_2. The (1×1) LEED pattern for the clean Cu(100) surface is shown in Fig. 6a. Exposing the (1×1) surface to Br_2 at 325 K immediately results in the formation of the $c(2\times2)$ pattern shown in Fig. 6b. This result is similar to those obtained previously for Cl_2 and Br_2 adsorption on the (100) surfaces of Cu and other fcc metals [8,10,26,27]. The only difference is that it had been reported that either higher adsorption temperatures or annealing above 425 K was required to observe a sharp $c(2\times2)$ pattern [26,27]. Here a sharp pattern was observed at 325 K and no noticeable temperature dependence was observed. X-ray scattering studies of Cl on Cu(100) showed that the $c(2\times2)$ pattern is due to Cl atoms adsorbed in four-fold hollows on the surface [26]. The fact that the Br $c(2\times2)$ saturates at doses similar to those required to saturate the desorption peaks associated with Br chemisorption suggests a similar origin for the Br $c(2\times2)$ pattern. Further, the observed $c(2\times2)$ pattern is visible immediately upon adsorption, indicating an attractive interaction between adsorbed Br atoms and sufficient mobility of adsorbed Br atoms at 325 K to form adsorbate islands.

Continued exposure to Br_2 at 325 K resulted in the LEED pattern shown in Fig. 6c. The same LEED pattern was obtained by subliming Cu_3Br_3 onto a $c(2\times2)$ layer of adsorbed Br atoms, as shown in Fig. 6d, suggesting that the pattern reflects an equilibrium surface at 325 K. It should be noted that the CuBr growth rates for both reaction and deposition were very slow (greater than 15 min were required to form the layers that gave the LEED patterns shown in Fig. 6c and 6d). The pattern can be viewed as the (1×1) pattern plus two equivalent hexagonal patterns separated by a 30° rotation. This pattern can be attributed to two rotationally equivalent domains of epitaxial (111) γ-CuBr (zinc blende structure) with the CuBr $[0\bar{1}1]$ direction parallel to the Cu [001] direction. Notice that Fig. 6 shows that the hexagonal spots coincide with the $c(2\times2)$ spots thus the periodicity of the CuBr layer in the $[0\bar{1}1]$ direction matches that of the $c(2\times2)$ layer. This gives a Br–Br distance of 3.62 Å in the CuBr layer, considerably smaller than the 4.02 Å distance in bulk CuBr [28]. The hexagonal pattern could also be due to the (0001) surface of β-CuBr. The in-plane periodicity of the (0001) surface of β-CuBr, however, is nearly identical to that of γ-CuBr (111) (4.06 Å

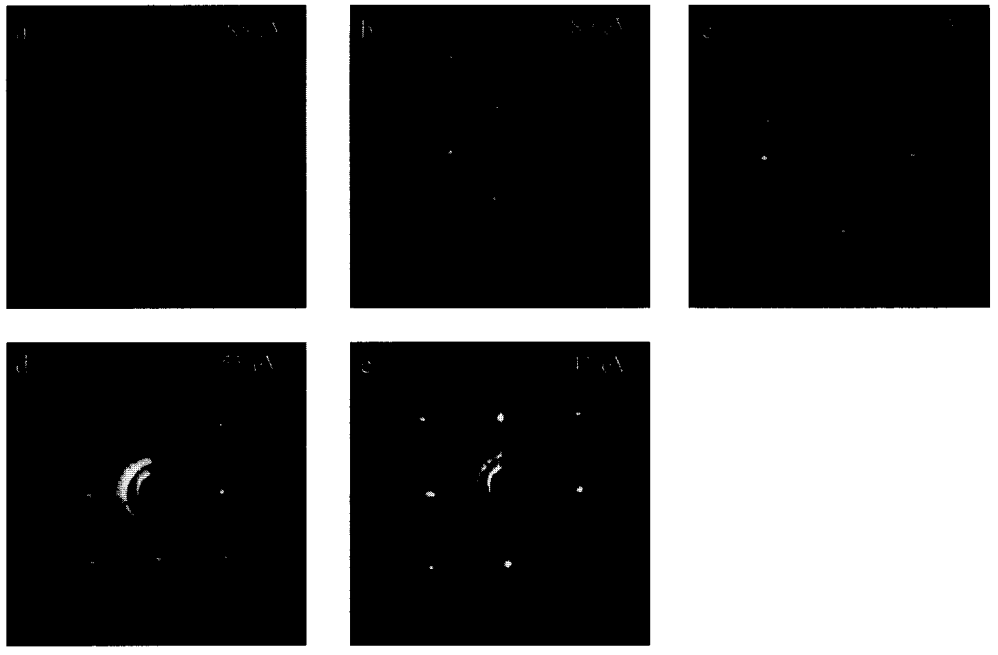

Fig. 6. Low-energy electron diffraction patterns illustrating structural changes due to the interaction of Br_2 with Cu(100): (a) (1×1) LEED pattern for clean Cu(100), (b) $c(2\times2)$ pattern observed immediately after adsorption of Br_2 at 325 K, (c) pattern observed after exposure to Br_2 dose of 30 000 μA s at 325 K, (d) pattern observed following vapor-phase deposition of CuBr film onto $c(2\times2)$ Br layer, and (e) $c(2\times2)$ pattern observed after 30 000 μA s Br_2 exposure and heating to 400 K. The patterns in (c) and (d) are attributed to two equivalent domains of epitaxial CuBr(111) separated by a 30° rotation.

versus 4.02 Å), so in either case the CuBr layer is under considerable compression.

The LEED patterns in Fig. 6c and 6d can also be viewed as the $c(2\times2)$ pattern plus two equivalent square patterns rotated $\pm30°$ from the $c(2\times2)$ pattern. However, there is no apparent benefit to forming a CuBr layer with square symmetry rotated 30° from the adsorbate layer, while the formation of hexagonal layers can be understood in several ways. First, the compressed hexagonal layer places many of the Cu atoms of the CuBr layer in high-coordination four-fold hollow sites of the adsorbed Br layer. In addition, Cu_3Br_3 is a six-membered ring [24] with a structure that can be pictured as the smallest possible (111) facet of the zinc blende structure. Therefore, when CuBr films are grown by depositing Cu_3Br_3, it is not surprising that (111)-oriented or hexagonal films form.

For a thin layer of hexagonal symmetry on top of a surface with square symmetry, additional spots in the LEED pattern due to multiple scattering are expected [29]. Fig. 7a illustrates the predicted positions of these spots for two equivalent domains of a (111) epitaxial layer with the $[0\bar{1}1]$ direction parallel to the [001] direction of the (100) substrate. In Fig. 7, the periodicity of the overlayer is $\sqrt{2}$ times the periodicity of the substrate. As shown in Fig. 7b, spots arising from multiple scattering of the first-order spots can be seen in the LEED pattern of CuBr formed by reaction of Br_2 with Cu(100). The lack of multiple scattering spots due to higher-order diffraction peaks suggests that the domain size of the epitaxial layer may not be large.

The temperature dependence of the structure of the CuBr layers was also studied. It was found that slowly heating the sample above 365 K decreases the intensity of the LEED patterns shown in Figs. 6c and 6d. When a temperature of 400 K was reached, only the $c(2\times2)$ pattern was observed, as shown in Fig. 6e (It should be noted that the disappearance of the LEED pattern was not due to the onset of Cu_3Br_3 desorption; TPD experiments following heating to 400 K revealed

(a)

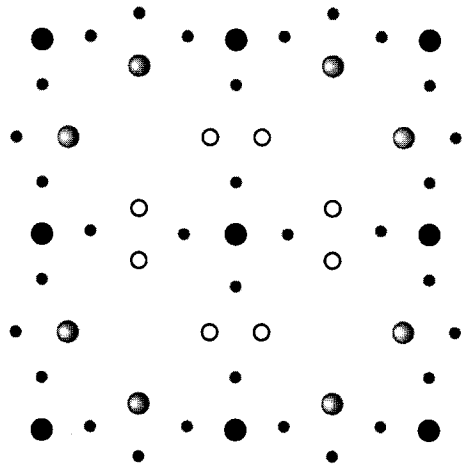

Single Scattering Spots
● Cu{100}c(2x2)-Br
◉ CuBr(111)

Multiple Scattering Spots
○ First Order
• Higher Order

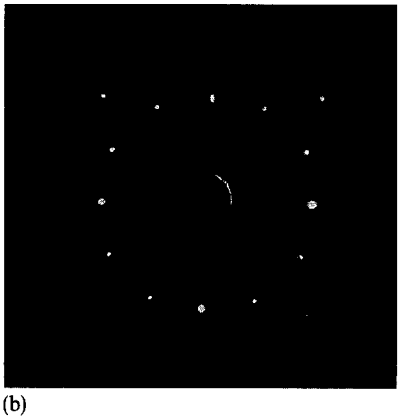

(b)

Fig. 7. (a) Schematic LEED pattern showing the multiple scattering spots expected for CuBr(111) on a c(2 × 2) surface structure. The large black circles represent the c(2 × 2) pattern, while the large shaded circles represent the CuBr(111) diffraction spots. The open circles represent diffraction spots resulting from first-order multiple scattering, while the small filled circles are due to higher-order multiple scattering. The LEED pattern in (b), obtained at 41 eV, shows the expected first-order multiple scattering diffraction spots for CuBr(111) formed by reaction of Br_2 with Cu(100).

no significant decrease in the CuBr coverage). Also, CuBr films formed above 365 K displayed only the c(2 × 2) pattern. These results are attributed to disordering of the CuBr film, presumably driven by relief of the compression of the CuBr layer. The TPD results suggest that the film transforms into a mixture of α and β CuBr. The transformation of the LEED pattern on annealing was irreversible. This does not mean that the structures formed at lower temperatures are not thermodynamically favored; reordering the film would require a many body process while the initial slow growth of the film requires only accommodation of individual CuBr or Cu_3Br_3 moieties.

3.3. Adsorption and reaction kinetics

The integral of a TPD curve yields the initial coverage. Thus by plotting the TPD peak integrals versus exposure, adsorption kinetics can be obtained. These data are shown in Fig. 8a for the desorption peaks associated with chemisorbed Br, and in Fig. 8b for the CuBr sublimation peaks. As shown in Fig. 8a, Br_2 initially chemisorbs on the Cu(100) surface with a constant sticking coefficient, the coverage of the chemisorbed layer increasing linearly with dose. Using the approximate value of 80 μA s L^{-1}, a sticking coefficient of 0.3 is obtained, close to the value reported for Cl_2 adsorption on Cu surfaces [7]. These data were obtained for a sample temperature of 325 K; in the chemisorption regime no significant temperature dependence on the adsorption rate was observed.

Once the chemisorbed layer is saturated, the sticking coefficient decreases greatly but does not go zero. Continued exposure to Br_2 populates the peaks associated with the formation of CuBr. As shown in Fig. 8b, the formation of CuBr does not begin until the chemisorbed layer is saturated and is characterized by a constant sticking coefficient. This result was independent of pressure over the range studied. Similar behavior has been observed for Cl_2 on Cu(100), although with a sticking coefficient roughly a factor of ten lower than for Br_2 [30]. As explained by Winters et al. [6] for Cl_2 on Cu(100), the linear growth of the halide layer indicates that the reaction is adsorption-rate limited [6]. If diffusion was a significant factor in determining the reaction rate, then the rate would be expected to decrease as the halide layer thickens. The data are also consistent with the place-

exchange regime of the Cabrera–Mott theory of oxidation [31].

The CuBr formation kinetics exhibit an interesting dependence on sample temperature during Br_2 exposure. This is shown in Fig. 9, where the integral of the CuBr sublimation peaks is plotted versus Br_2 exposure for three different cases: (i) sample temperature held at 325 K, (ii) sample temperature held at 375 K, and (iii) annealing the chemisorbed c(2×2) layer to ~650 K and then dosing with the sample at 325 K. Fig. 9 shows that annealing the sample or changing the sample temperature does not change the reaction mechanism, since all three curves are linear. However, annealing the chemisorbed layer increases the sticking coefficient while increasing the sample temperature during dosing decreases the sticking coefficient. The annealing effect was irreversible. Annealing was found to produce no noticeable changes in the LEED pattern of the chemisorbed layer, although TPD indicated a slight increase in the amount of Br chemisorbed in the 870 K peak when annealed samples were dosed again at lower temperatures. The increase in the amount of Br chemisorbed can be attributed to annealing increasing the domain size and decreasing the defect density of the c(2×2) layer. Though one might expect this to decrease the CuBr formation rate and not increase it, STM studies of Ni oxidation showed that such decreases in defect density do not affect oxidation rates [32].

The temperature dependence was further investigated by varying the surface temperature for a constant dose of 10 000 μA s and measuring the amount of Cu_3Br_3 that desorbs. These data are shown in Fig. 10 for clean Cu(100) surfaces and for surfaces with an annealed chemisorbed c(2×2) Br layer. In Fig. 10 the data are normalized to the sublimation peak integral for dosing at 325 K for each case. The annealed layer displays a decrease in the amount of Cu_3Br_3 desorbed throughout the temperature range studied and the data suggest a steeper decrease with temperature above 365 K. This decrease is not due to the onset of desorption during Br_2 exposure; surfaces annealed to temperatures up to 400 K showed no significant loss of CuBr in subsequent TPD experiments. When these experiments were performed on the clean Cu(100) surface, the amount of Cu_3Br_3 desorbing was observed to initially increase with temperature, then decrease above 365 K. The initial increase in the clean Cu(100) curve may be due to the same annealing effect previously mentioned. Since the decrease in the amount of Cu_3Br_3 desorbed occurs in the same temperature range as the change in the LEED pattern from a hexagonal structure to a structure with no long-range order, it is tempting to attribute the decrease in reactivity to a structural change in the surface. However, the change in the LEED pattern was irreversible, while the decreases in reactivity shown in Fig. 10 were reversible. Further, when a CuBr layer with no long-range order, formed by either adsorbing Br_2 at 385 K or by annealing an ordered layer to 400 K, was exposed to Br_2 at 325 K, the additional adsorption occurred with a sticking coefficient characteristic of the lower dosing temperature.

4. Discussion

The results for Br_2 on Cu(100) share many of the same general features with previous results for Cl_2. In both cases the halogen initially adsorbs into a chemisorbed state with a high sticking coefficient to form a c(2×2) layer, and continued exposure results in the slow linear growth of a halide layer. Etching then occurs by sublimation of the halide layer. Although there are similarities between the interaction between Cl_2 and Br_2 and Cu(100) there are also significant differences that make Br_2 a potentially more attractive etchant. Bromine is far more reactive towards Cu, and thus it is less likely that steady-state etching will be limited by the halide formation rate. Therefore, for Br_2 it should be easier to achieve etching rates limited only by the vapor pressure of the halide (the vapor pressures of bulk CuCl and CuBr are comparable, so this is not an issue). Moreover, the low-temperature desorption peak observed at low CuBr coverages indicates that Br_2 etching temperatures may not be limited by the vapor pressure of bulk CuBr. No similar low-temperature desorption peaks have been observed for Cl_2 on Cu [6,30]. Fig. 5 shows that the low-temperature desorption peak results in sublimation rates comparable to bulk CuBr at temperatures at least 25

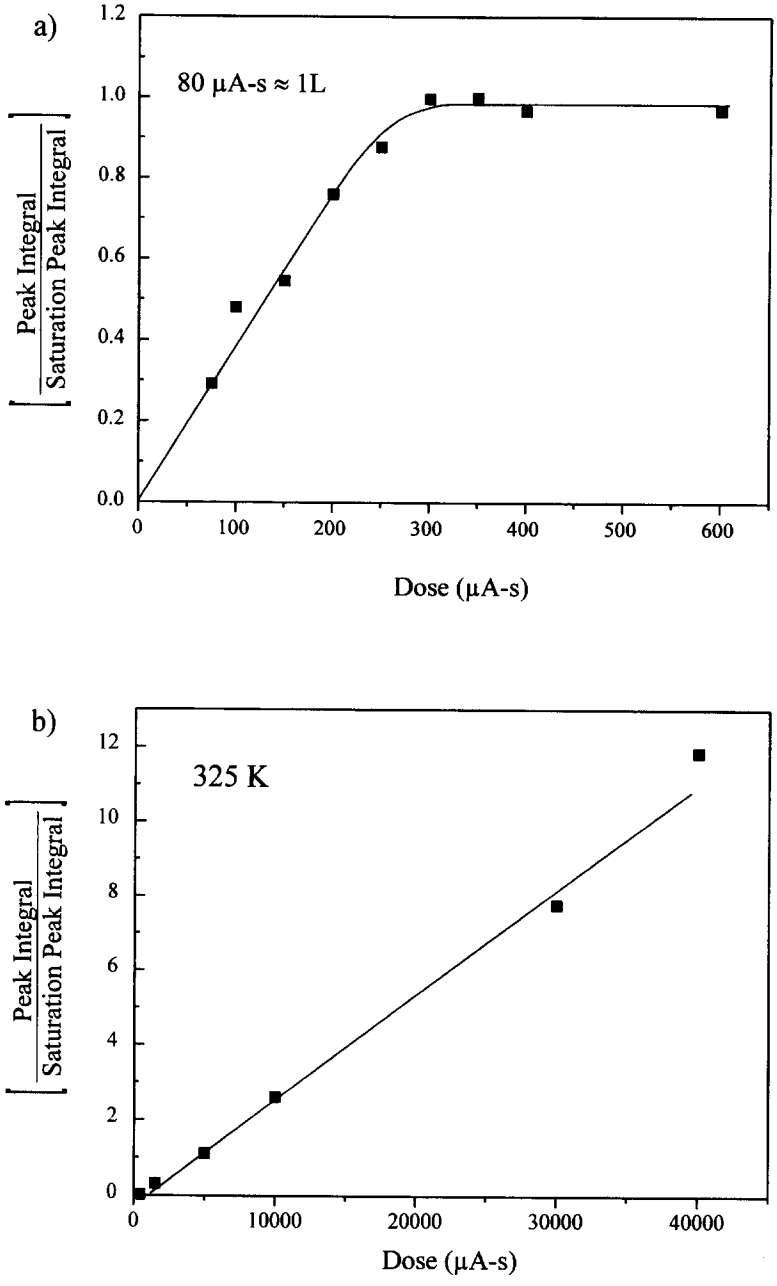

Fig. 8. Plots of adsorption uptake versus Br_2 dose at 325 K for (a) chemisorption of Br_2, obtained by integrating the CuBr desorption peaks above 650 K, and (b) reaction of Br_2 to CuBr, obtained by integrating the Cu, CuBr, and Cu_3Br_2 desorption peaks below 650 K. The data in both (a) and (b) are normalized to the integral of the chemisorption peaks at saturation. The plots show that growth of bulk CuBr does not begin until after the chemisorbed layer is saturated.

K lower. Obviously this alone is not sufficient to result in lower etching temperatures. For that to occur, the low-temperature peak must not be limited to the (100) orientation, the low-temperature peak must persist as the surface is etched, and it must be possible to control the thickness of the

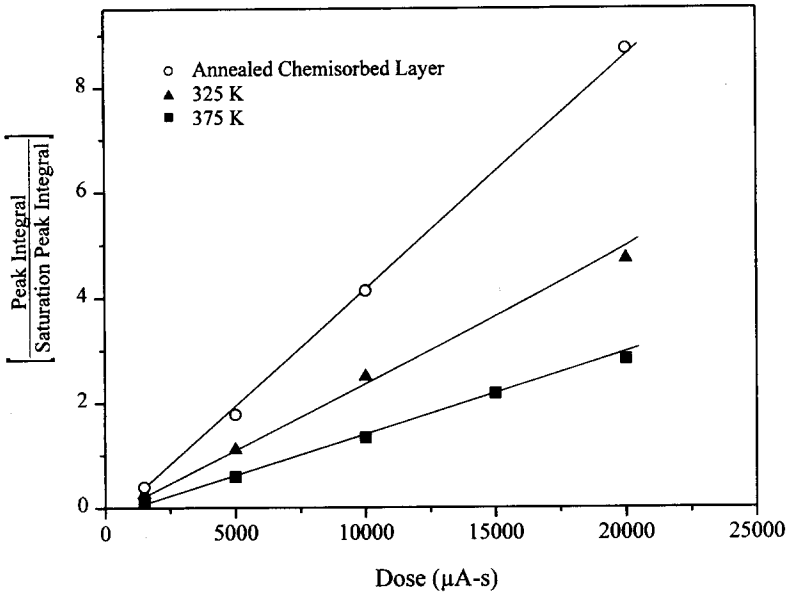

Fig. 9. The amount of desorbing Cu_3Br_3, obtained by integrating the Cu, CuBr and Cu_3Br_2 desorption peaks below 650 K, as a function of dose for dosing at 325 K, at 375 K, and for dosing a c(2 × 2) Br layer annealed to 650 K at 325 K. All data are normalized to the integral of the chemisorption peak at saturation for the clean Cu(100) sample dosed at 325 K.

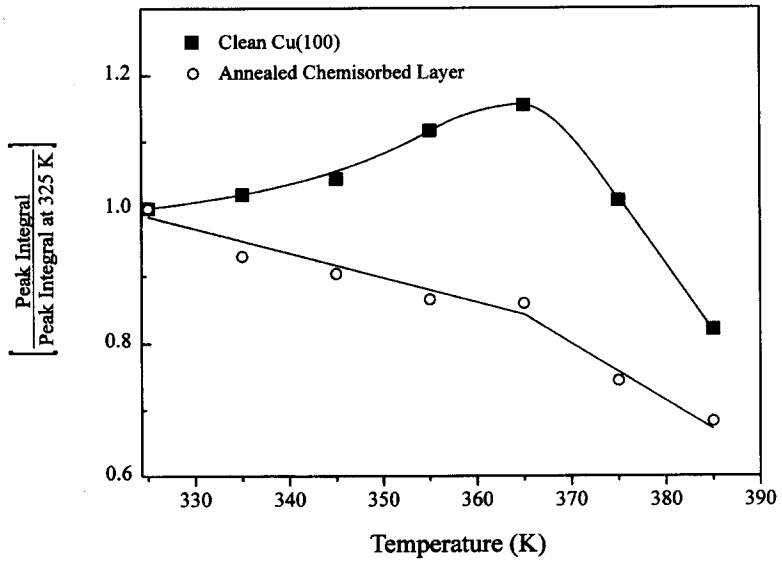

Fig. 10. Dependence of the Cu_3Br_3desorption yield as a function of exposure temperature at a constant dose of 10,000 μA s for a c(2 × 2) Br layer annealed to 650 K and for a non-annealed surface. Each curve is normalized to its respective TPD peak integral obtained at 325 K

halide layer since the low-temperature peak is not observed for thick halide films. We are currently investigating these issues.

Halogenation reactions can be categorized as oxidation reactions [33], therefore the results obtained for bromination of Cu are also relevant

to oxidation of metals and corrosion. Decreases in reaction rate with temperature have been observed for other oxidation reactions [10–17] including the reaction of Cl_2 with Cu(100) [6]. The best characterized example of such behavior is the oxidation of Ni(100) [13–17,34–36]. The oxidation of Ni(100) shows some similarities to the bromination of Cu(100); oxygen forms a $c(2\times2)$ chemisorbed layer on Ni(100) and epitaxial NiO(111) has been observed (albeit rocksalt structure versus the zinc blende or wurtzite structure of CuBr) [13,14,16,34–36]. Scanning tunneling microscopy studies have shown that the decrease in oxidation rate of Ni(100) with sample temperature is associated with structural changes in the surface [32]. At low temperatures, NiO nucleates at step edges while increasing the temperature causes the step edges to facet, yielding them unreactive. The NiO must then nucleate on the terraces, which is a much slower process. This suggests irreversible temperature effects for oxidation of Ni(100). This model could possibly be generalized to explain the increase in the CuBr formation rate when the chemisorbed layer is annealed if the step faceting in this case increases the reactivity of the steps towards Br_2. We plan to investigate this possibility using STM. The reversible decrease in the CuBr formation rate for the annealed chemisorbed layer, however, depends solely on the reaction temperature and cannot be understood in terms of irreversible structural changes in the surface. We have made similar observations for the reaction of Cl_2 on Cu(100), suggesting that this is not unique to Br_2 on Cu(100) [30]. Obviously, further study is required to determine if this is a general feature of oxidation reactions and to determine the origin of the effect.

5. Summary

The etching of Cu(100) by Br_2 was characterized using TPD and LEED. It was shown that the general etching mechanism is a two-step process: (i) reaction to form CuBr, and (ii) removal of CuBr by sublimation. Each of these steps was systematically characterized. Bromine was found to initially adsorb onto Cu surfaces with a high sticking coefficient, forming a strongly bound $c(2\times2)$ adsorbate layer. After the adsorbate layer was saturated, the sticking coefficient was observed to decrease greatly, but did not go to zero. Rather, continued Br_2 exposure resulted in the growth of CuBr. At 325 K, CuBr grown both by vapor deposition and by reaction with Br_2 exhibited hexagonal LEED patterns attributed to compressed epitaxial CuBr(111). Annealing to 400 K was observed to destroy any long-range order in the CuBr films. The growth of CuBr was also characterized by a constant sticking coefficient, indicating that over the range studied diffusion does not play a role in determining the reaction rate. The reaction to form CuBr was shown to depend on temperature in two distinct ways. Annealing the $c(2\times2)$ adsorbate layer was found to irreversibly increase the reaction rate, while a reversible decrease in reaction rate was observed with increasing reaction temperature. The first effect was attributed to thermally induced structural changes in the chemisorbed layer, while the second effect remains poorly understood. Sublimation of the CuBr layer was observed to depend strongly on the CuBr coverage. At high coverages, zero-order desorption was observed with an activation energy for desorption consistent with sublimation of α-CuBr. At low CuBr coverages, a low-temperature desorption peak at 450 K was observed that could not be explained in terms of sublimation of any of the bulk phases of CuBr. The same peak was observed whether the CuBr was formed by reaction or by deposition, indicating, along with the LEED results, that the desorption process is independent of the formation process, that the low-temperature peak is associated with sublimation of CuBr, and suggesting that the reaction of Br_2 with Cu(100) produces near-equilibrium structures. Further, the results suggest that by limiting the thickness of the CuBr layer, etching temperatures can be reduced below those anticipated from consideration of bulk vapor-pressure data.

Acknowledgements

The authors acknowledge the assistance of V.M. Phanse and G. Zheng in carrying out this work.

The authors also thank V.E. Henrich for his helpful discussions concerning the LEED data. This work was supported by the National Science Foundation under grant numbers DMR-9414404 and CTS-9411568 (equipment).

References

[1] S.P. Murarka, Metallization: Theory and Practice for VLSI and ULSI (Butterworth-Heinemann, Boston, 1993).
[2] S. Wolf and R.N. Tauber, Silicon Processing for the VLSI Era, Vol. 1, Process Technology (Lattice Press, Sunset Beach, 1986).
[3] See MRS Bull. 18 (1993) No. 6, and MRS Bull. 19 (1994) No. 8, both issues devoted to Cu metallization.
[4] H.F. Winters and J.W. Coburn, J. Vac. Sci. Technol. B 3 (1985) 1376.
[5] H.F. Winters, J. Vac. Sci. Technol. B 3 (1985) 9.
[6] H.F. Winters, J. Vac. Sci. Technol. A 3 (1985) 786.
[7] S. Park, T.N. Rhodin and L.C. Rathbun, J. Vac. Sci. Technol. A 4 (1986) 168.
[8] N.V. Richardson and J.K. Sass, Surf. Sci. 103 (1981) 496.
[9] T.J. Chuang and W. Sesselmann, Surf. Sci. 176 (1986) 32.
[10] M. Kitson and R.M. Lambert, Surf. Sci. 100 (1980) 368.
[11] M. Bowker and K.C. Waugh, Surf. Sci. 134 (1983) 639.
[12] A.L. Linsebigler, V.S. Smentkowski, M.D. Ellison and J.T. Yates, Jr., J. Am. Chem. Soc. 114 (1992) 465.
[13] P.H. Holloway and J.B. Hudson, Surf. Sci. 43 (1974) 123.
[14] D.F. Mitchell, P.B. Sewell and M. Cohen, Surf. Sci. 61 (1976) 355.
[15] P.H. Holloway, J. Vac. Sci. Technol. 18 (1981) 653.
[16] W.D. Wang, N.J. Wu and P.A. Thiel, J. Chem. Phys. 92 (1990) 2025.
[17] M. Bäumer, D. Cappus, H. Kuhlenbeck, H.-J. Freund, G. Wilhelmi, A. Brodde and H. Neddermeyer, Surf. Sci 253 (1991) 116.
[18] J. Farkas, K.M. Chi, M.J. Hampden-Smith, T.T. Kodas and L.H. Dubois, J. Appl. Phys. 73 (1993) 1455.
[19] M.J. Hampden-Smith and T.T. Kodas, MRS Bull. 18(6) (1993) 39.
[20] M. Chander, D.A. Goetsch, C.M. Aldao and J.H. Weaver, Phys. Rev. B 52 (1995) 8288.
[21] N.D. Spencer, P.J. Goddard, P.W. Davies, M. Kitson and R.M. Lambert, J. Vac. Sci. Technol. A 1 (1983) 1554.
[22] B. Kasemo and L. Walldén, Surf. Sci. 53 (1975) 393.
[23] A.J. Shelton, Trans. Faraday Soc. 57 (1961) 2113.
[24] P.J. Goddard and R.M. Lambert, Surf. Sci. 67 (1977) 180.
[25] J.T. Yates, Jr., in: Methods of Experimental Physics 22, Eds. R.L. Park and M.G. Lagally (Academic, Orlando, 1985), pp. 425–464.
[26] P.H. Citrin, D.R. Hamann, L.F. Mattheis and J.E. Rowe, Phys. Rev. Lett. 49 (1982) 1712.
[27] E. Zanazzi, F. Jona, D.W. Jepsen and P.M. Marcus, Phys. Rev. B 14 (1976) 432.
[28] A. Goldmann, Phys. Status Solidi B 81 (1977) 9.
[29] E. Bauer, Surf. Sci. 7 (1967) 351.
[30] C.Y. Nakakura, V.M. Phanse and E.I. Altman, to be published.
[31] F.P. Fehlner and N.F. Mott, Oxid. Metals 2 (1970) 59.
[32] E. Kopatzki and R.J. Behm, Phys. Rev. Lett. 74 (1995) 1399.
[33] H.F. Winters, J.W. Coburn and T.J. Chuang, J. Vac. Sci. Technol. B 1 (1983) 469.
[34] G. Dalmai-Imelik, J.C. Bertolini and J. Rousseau, Surf. Sci. 63 (1977) 67.
[35] R.S. Saiki, A.P. Kaduwela, M. Sagurton, J. Osterwalder, D.J. Friedman, C.S. Fadley and C.R. Brundle, Surf. Sci. 282 (1993) 33.
[36] D.L. Wareen and P.A. Thiel, J. Chem. Phys. 100 (1994) 659.